JOURNAL OF SOLID STATE CHEMISTRY **132,** 41–46 (1997)
ARTICLE NO. SC977404

A V(IV) Tetraphosphate with a Tunnel Structure $K_2(VO)_2P_4O_{13}$

M. M. Borel, A. Leclaire, J. Chardon, J. Provost, H. Rebbah,* and B. Raveau

Laboratoire CRISMAT, URA 1318 associée au CNRS, ISMRA et Université de Caen, 6, Boulevard du Maréchal Juin, 14050 Caen Cedex, France; and
**Laboratoire de cristallographie et cristallogenèse, Institut de Chimie, USTHB BP 32, El Alia Bab Ezzouar, Alger, Algeria*

Received December 2, 1996; in revised form March 24, 1997; accepted April 2, 1997

A V(IV) tetraphosphate $K_2(VO)_2P_4O_{13}$ has been synthesized for the first time, and crystals of this new phase can be grown in air. It crystallizes in the space group *Pbca* with $a = 22.181(2)$Å, $b = 11.564(1)$Å, $c = 9.948(1)$Å. The original structure of this phase consists of corner sharing P_4O_{13} tetraphosphate groups and VO_6 octahedra forming a tridimensional framework $[V_2P_4O_{15}]_\infty$. The latter delimits large tunnels running along c and small tunnels running along b and [1 0 1], where two kinds of sites K(1) and K(2) are occupied by potassium. The horseshoe conformation of the P_4O_{13} group is different from those observed previously which are principally S shaped. The magnetic susceptibility investigation shows a paramagnetic behavior, with a *C* parameter of 1.55 μ_B. The thermogravimetric study shows the exceptional stability of V(IV) in this phosphate matrix, whatever the atmosphere air or oxygen up to 750°C.

INTRODUCTION

Recent studies of vanadium phosphates have shown that it is possible to isolate a large number of original structures (see for a review Refs. (1, 2)), due to the various oxidation states of vanadium and to the ability of this element to adopt different coordinations (octahedral, pyramidal, and tetrahedral).

Numerous vanadium monophosphates and diphosphates are known, some of which are of great interest for their redox catalytic properties. By contrast, the number of vanadium polyphosphates that have been identified to date is very limited. No V(IV) and V(V) anhydra polyphosphates are actually known, whereas only four V(III) polyphosphates have been synthesized, $V(PO_3)_3$ (3), $CsV_2P_5O_{16}$ (4), $KV_4(PO_4)(P_2O_7)(P_4O_{13})$ (5), and $V_6Si_2O_7(PO_3)_6(P_4O_{13})$ (6).

The difficulty in synthesizing vanadium polyphosphates arises from the fact that the amount of phosphorus required for these materials (P : V generally ≥ 2), which is greater than that needed for monophosphates or diphosphates, may favor the formation of glasses when working at high temperature. Thus soft chemistry methods are of great interest toward generating new materials in this field. Among them, hydrothermal synthesis has been extensively used for the synthesis of microporous phosphates. Such a method allows large organic cations to be interpolated at low temperature and polycations, like Keggin ions, to be stabilized, but most of the time it does not allow anhydra or hydroxyl group free polyphosphates to be grown as single crystals. In the present study, we adopt a different strategy for the crystal growth of reduced vanadium phosphates, based on the fact that they can be grown in air provided one of the reactants is a reducing agent and is very reactive, so that a low temperature can be used. We report herein on a new V(IV) tetraphosphate, $K_2(VO)_2P_4O_{13}$, with an original tunnel structure; on its stability in an oxygen atmosphere; and on its magnetic behavior.

EXPERIMENTAL

Strategy of Crystal Growth

In order to get a chance to grow single crystals of a new phase in the system K–V–P–O, involving polyphosphate groups, a systematic investigation of compositions involving mixtures of K_2CO_3, V_2O_5, $H(NH_4)_2PO_4$ was performed, fixing the V : P molar ratio to 1/2 and varying the K : P + V ratio between 1/4 and 1/2. In the same way the temperature was scanned from 400 to 600°C. Positive results were obtained for the nominal mixture "K_2CO_3, V_2O_5, $4H(NH_4)_2PO_4$" for 2 h, and the mixture was reground and heated at 550°C and finally quenched to room temperature.

Under these conditions, blue-green crystals were extracted from a green polycrystalline mixture.

Chemical Synthesis

Attempts to prepare a pure polycrystalline phase were made after the results of the single crystal study and of EDS analysis that indicated the composition $K_2V_2P_4O_{15}$.

The synthesis was carried out in two steps. First, an intimate mixture of K_2CO_3 and $H(NH_4)_2PO_4$ in the molar ratio 1 : 4 was heated in air to 400°C in a platinum crucible to eliminate CO_2, NH_3, and H_2O. Then the appropriate

0022-4596/97 $25.00

amount of a mixture of V_2O_5 and V in the molar ratio 1.6 : 0.4 was added and the finely ground mixture was sealed in a silica ampoule. The latter was heated for 12 h at 650°C and then cooled at a rate of 20°C h^{-1} to room temperature.

The result was a blue turquoise powder. The powder X-ray diffraction pattern of the latter was indexed in an orthorhombic cell in agreement with the parameters obtained from the single crystal X-ray study.

Energy Dispersive Analysis

The elementary analysis of the elements K, V, P was performed with a Tracor microprobe mounted on a scanning electron microscope; this allowed the "K V P_2" composition to be established in agreement with the structure determination.

X-Ray Diffraction Study

Different crystals were tested by the Weissenberg method using Cu$K\alpha$ radiation.

A blue-green crystal with dimensions $0.064 \times 0.038 \times 0.038\ mm^3$ was selected for structure determination. The cell parameters were determined by diffractometric techniques at 25 °C with a least square refinement based upon 25 reflections with $18° < \theta < 22°$. The data were collected on a CAD4 ENRAF NONIUS diffractometer with the parameters reported in Table 1. The systematic extinctions $k = 2n + 1$ for $0kl$, $l = 2n + 1$ for $h0l$, and $h = 2n + 1$ for $hk0$ are consistent with the space group *Pbca*. The reflections were corrected for Lorentz polarization effects and for absorption. The structure was solved with the heavy atom method.

With regard to the refinement of the atomic coordinates, their anisotropic thermal parameters led to $R = 0.043$ and $R_w = 0.035$ an to the atomic parameters given in Table 2.

TABLE 1
Summary of Crystal Data, Intensity Measurements, and Structure Refinement Parameters for $K_2(VO)_2(P_4O_{13})$

1. Crystal data	
Space group	*Pbca*
Cell dimensions (Å)	$a = 22.181(2)$
	$b = 11.564(1)$
	$c = 9.548(1)$
Volume(Å)^3	2449.0(4)
Z	8
2. Intensity measurements	
λ(Mo$K\alpha$)	0.71073
Scan mode	$\omega - \theta$
Scan width (°)	$1.2 + 0.35\ \mathrm{tn}\,\theta$
Slit aperture (mm)	$1.1 + \mathrm{tn}\,\theta$
max θ(°)	45
Standard reflections	3 measured every 3600 s
Reflections with $I > 3\sigma$	997
3. Structure solution and refinement	
Parameters refined	113
Agreement factors	$R = 0.043\ R_w = 0.035$
Weighting scheme	$w = 1/\sigma^2$
Δ/σ max	<0.0005

TABLE 2
Atomic parameters of $K_2(VO)_2(P_4O_{13})$

Atom	x	y	z	B_{eq}
V(1)	0.0304(1)	0.1198(2)	0.2578(2)	0.51(5)
V(2)	0.22498(9)	− 0.0687(2)	− 0.0163(2)	0.60(5)
P(1)	0.0299(1)	0.3814(3)	0.1254(3)	0.52(6)
P(2)	0.1131(1)	0.5596(2)	0.2191(3)	0.44(6)
P(3)	0.3086(1)	0.1510(2)	− 0.0201(3)	0.47(6)
P(4)	0.1675(1)	0.0270(2)	0.2708(3)	0.46(6)
K(1)	− 0.0619(1)	0.1544(2)	− 0.0661(3)	1.42(8)
K(2)	0.1351(1)	0.1998(2)	− 0.0365(3)	1.61(9)
O(1)	0.0361(4)	0.0856(6)	0.0959(7)	1.1(2)
O(2)	0.0204(3)	− 0.0394(6)	0.3326(7)	0.8(2)
O(3)	0.1190(3)	0.1151(6)	0.2973(7)	0.6(2)
O(4)	0.0416(3)	0.2917(6)	0.2393(8)	0.6(2)
O(5)	− 0.0608(3)	0.1418(5)	0.2559(8)	0.7(2)
O(6)	0.0239(3)	0.1714(5)	0.4821(7)	0.5(2)
O(7)	0.2759(3)	− 0.1166(7)	0.0824(7)	1.2(2)
O(8)	0.2712(3)	− 0.0729(6)	− 0.1950(7)	0.8(2)
O(9)	0.1626(3)	− 0.0253(6)	0.1262(8)	0.7(2)
O(10)	0.1839(3)	− 0.2240(6)	− 0.0516(8)	0.6(2)
O(11)	0.2459(3)	0.1038(5)	− 0.0141(7)	0.8(2)
O(12)	0.1446(3)	− 0.0163(6)	− 0.1557(7)	0.7(2)
O(13)	0.0915(3)	0.4573(6)	0.1211(8)	0.6(2)
O(14)	0.3410(3)	0.1299(7)	0.1257(8)	1.1(2)
O(15)	0.3470(3)	0.0796(6)	− 0.1249(8)	0.6(2)

Note. Anisotropically refined atoms are given in the form of the equivalent isotropic displacement parameter defined as $B = \frac{4}{3}\sum_i\sum_j \mathbf{a}_i \cdot \mathbf{a}_j \cdot \beta_{ij}$.

Thermogravimetric Analysis in Air and Oxygen

Microthermogravimetric analysis was performed in air, and in oxygen, using a Setaram microbalance, by heating the sample up to 750° at a speed of 150°C h^{-1}.

Magnetic Measurements

The magnetic susceptibility of powdered samples was investigated by SQUID magnetometry in the 4.5–350 K temperature range. The zero field cooled magnetic moment of the sample was measured in a field of 1 tesla. The magnetic moment of the sample holder was measured in the same temperature range under the same magnetic field. The sample holder moment was then substracted from the measured total moment.

RESULTS AND DISCUSSION

Description of the Structure

The projection of the $[V_2P_4O_{15}]_\infty$ tridimensional framework along **c** (Fig. 1) shows that the latter consists of isolated VO_6 octahedra interconnected through tetraphosphate groups P_4O_{13}. These polyhedra delimit seven-sided tunnels running along *c* where the potassium cations are located.

The structure can be easily described by considering that it is built up of identical $[V_2P_4O_{17}]_\infty$ layers parallel to (0 1 0) that are one octahedron thick (Fig. 1). The projection of such a layer along **b** is shown in Fig. 2. The layer consists of identical $[V_2P_4O_{18}]_\infty$ ribbons running along [1 0 1]. Within each ribbon, the VO_6 octahedra form rows running along [1 0 1] where one V(1) octahedron alternates with one V(2) octahedron. Each ribbon is composed of two octahedral rows. Each P_4O_{13} group exhibits a snail-shell-like shape and ensures the connection between four successive octahedra (2 V(1) + 2 V(2)) of a double row of octahedra. Each extreme diphosphate group of the P_4O_{13} group (P(1)–P(2)–P(3)–P(4)) shares two apices with the same VO_6 octahedron (Fig. 2), forming VP_2O_{11} units (see Fig. 2, inset) already observed in many transition metal diphosphates (1). In this way, the V(2) octahedra are connected to the diphosphate groups "P(3)–P(4)," whereas the V(1) octahedra are associated with the diphosphate groups "P(1)–P(2)" (Fig. 2). Note that the diphosphate group "P(2)–P(3)" located in the middle of the P_4O_{13} group ensures the connection between two V(2) octahedra of two different rows, whereas two identical octahedra V(1) or V(2) are also linked along **c** through single PO_4 tetrahedra, P(1) and P(4), respectively. It is also remarkable that two successive P_4O_{13} groups along [1 0 1] are "fixed" on the same pair of V(1) octahedra and that their tetrahedra are "running" clockwise, from P(1) to P(4), forming an S-shaped tetrahedral entity. By contrast, the next S-shaped tetrahedral "P8" entity along [1 0 1] is anticlockwise oriented.

Each $[V_2P_4O_{18}]_\infty$ ribbon is connected to the next one along *c* through the apices of the P(4) and V(2) polyhedra: one PO_4 tetrahedron of one ribbon shares one apex with one VO_6 octahedron of the next ribbon. This results in the formation of S-shaped windows and five-sided windows (Fig. 2). The free oxygen apices of the VO_6 octahedra, V(1) and V(2), are located at the border of these windows.

Along *b*, two successive identical $[V_2P_4O_{17}]_\infty$ layers are deduced independently of each other by a *c* mirror. They share the corners of their polyhedra, P(3) and P(1) with V(2) and V(1), respectively, forming the tridimensional framework $[V_2P_4O_{15}]_\infty$.

The view of the structure along *b* (Fig. 3) and along [1 0 1] (Fig. 4) shows the existence of tunnels running along those directions. Nevertheless the size of these tunnels is rather small, so it cannot be considered an actual intersecting tunnel structure. Consequently no mobility can be expected for the K^+ cations in this structure, in agreement with the normal thermal factors observed for these cations (Table 2).

The interatomic distances (Table 3) show for the PO_4 tetrahedra a regular geometry. The terminal P(1) and P(4)

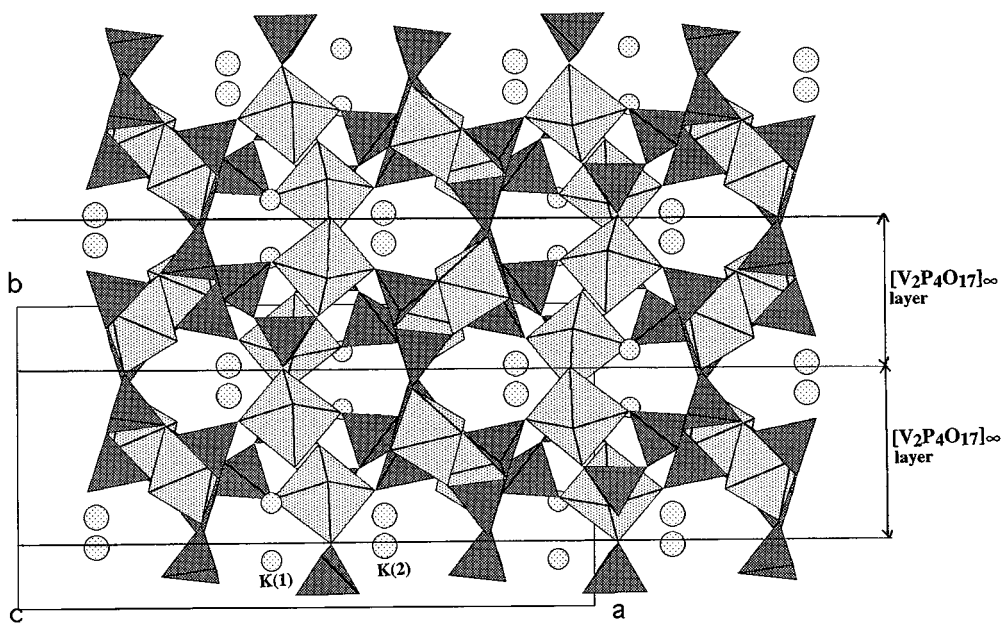

FIG. 1. Projection of the structure of $K_2(VO)_2(P_4O_{13})$ along *c*.

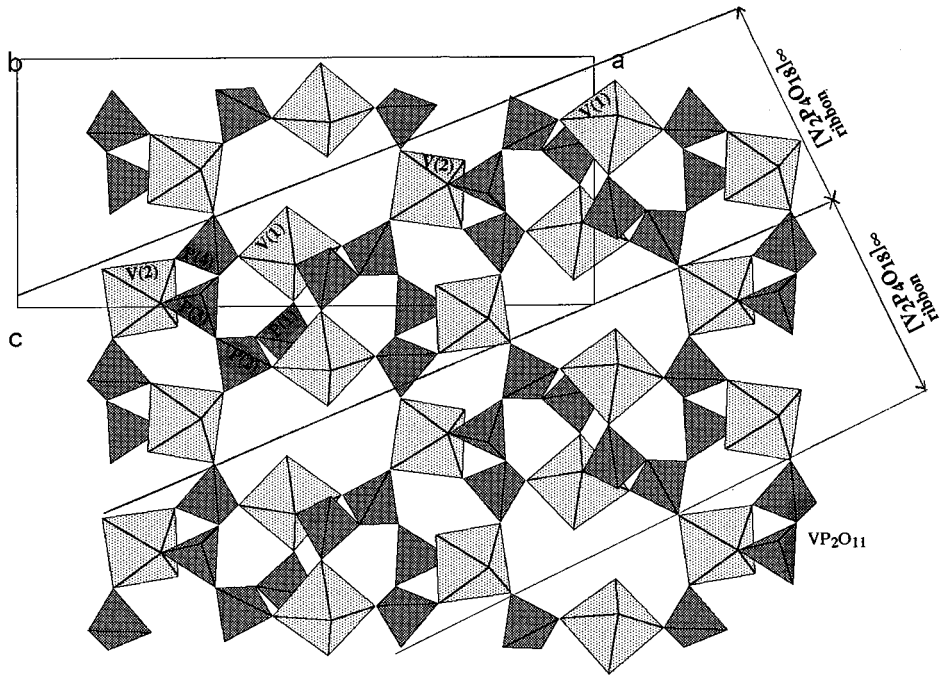

FIG. 2. Projection of a layer $[V_2P_4O_{17}]_\infty$ along *b*.

tetrahedra that form the P_4O_{13} group exhibit three short P–O distances (1.496–1.525 Å) corresponding to P–O–V bonds and a longer P–O distance (1.617–1.624 Å) characteristic of the P–O–P bond in diphosphate groups. The P(2) and P(3) intermediate tetrahedra are characterized by two short P–O distances (1.474–1.518 Å) and two longer P–O distances (1.551–1.586 Å) corresponding to P–O–V and P–O–P bonds, respectively. Most interesting is the horseshoe-like configuration of the P_4O_{13} groups (Fig. 5a) that is characterized by two extreme bridging P–O–P angles of 130–133.9° and an intermediate angle of 150.1°. This geometry is very different from that of $KV_4(PO_4)(P_2O_7)(P_4O_{13})$ (5), whose P_4O_{13} unit exhibits an S-shaped configuration (Fig. 5b) with three P–O–P bridging angles very close to one another, ranging from 132.5 to 135.3°. Although not identical, the tetraphosphates $Mo_2O_2P_4O_{13}$ (7) and

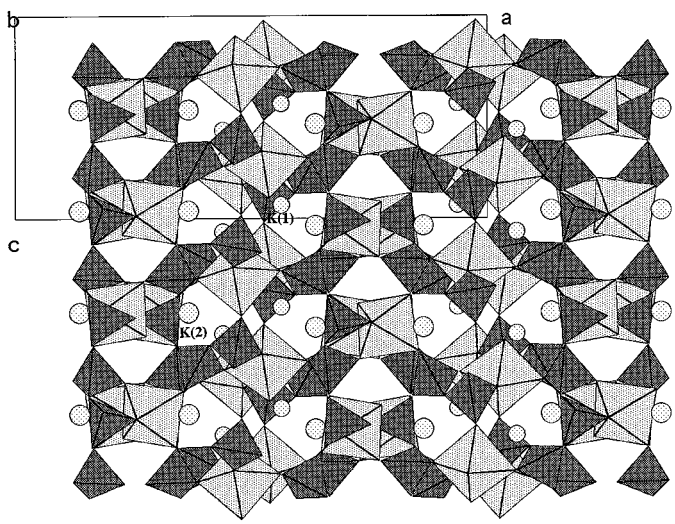

FIG. 3. Projection of the structure of $K_2(VO)_2(P_4O_{13})$ along *b*.

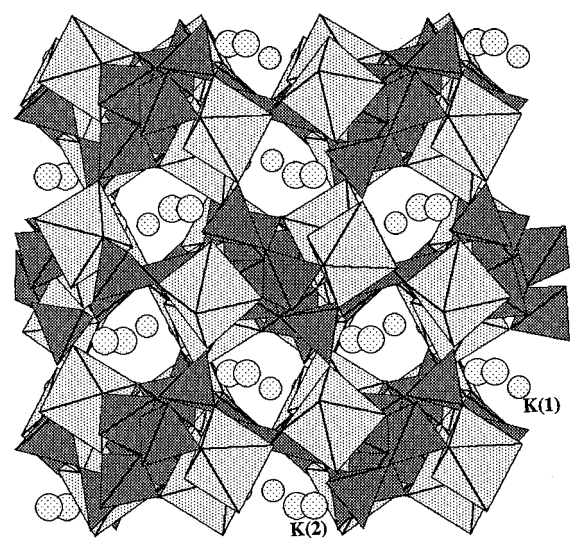

FIG. 4. Projection of the structure of $K_2(VO)_2(P_4O_{13})$ along [1 0 1].

TABLE 3
Distances (Å) and Angles (°) in the Polyhedra

V(1)	O(1)	O(2)	O(3)	O(4)	O(5)	O(6)
O(1)	**1.601(7)**	2.71(1)	2.68(1)	2.75(1)	2.72(1)	3.83(1)
O(2)	97.3(4)	**1.987(7)**	2.84(1)	3.96(1)	2.86(1)	2.82(1)
O(3)	95.6(4)	90.9(3)	**2.002(7)**	2.72(1)	4.02(1)	2.82(1)
O(4)	98.6(4)	164.0(3)	85.5(3)	**2.011(7)**	2.86(1)	2.73(1)
O(5)	95.8(4)	90.5(3)	168.3(3)	89.9(3)	**2.039(7)**	2.88(1)
O(6)	178.5(4)	84.0(3)	83.6(3)	80.1(3)	84.9(3)	**2.227(7)**
V(2)	O(7)	O(8)	O(9)	O(10)	O(11)	O(12)
O(7)	**1.572(8)**	2.70(1)	2.76(1)	2.71(1)	2.79(1)	3.87(1)
O(8)	97.8(4)	**1.991(7)**	3.94(1)	2.95(1)	2.73(1)	2.91(1)
O(9)	100.2(4)	160.6(3)	**2.005(7)**	2.90(1)	2.73(1)	2.72(1)
O(10)	96.3(4)	93.8(3)	91.4(3)	**2.041(7)**	4.05(1)	2.74(1)
O(11)	100.1(4)	85.2(3)	84.6(3)	163.6(6)	**2.048(7)**	2.97(1)
O(12)	173.9(4)	84.8(3)	78.0(3)	77.9(3)	85.7(3)	**2.305(7)**
P(1)	O(2)^{i}	O(4)	O(6)^{ii}	O(13)		
O(2)^{i}	**1.499(8)**	2.49(1)	2.54(1)	2.52(1)		
O(4)	110.6(4)	**1.525(8)**	2.52(1)	2.48(1)		
O(6)^{ii}	115.1(4)	112.9(4)	**1.504(8)**	2.50(1)		
O(13)	107.6(4)	104.1(4)	105.7(4)	**1.624(8)**		
P(2)	O(13)	O(5)^{i}	O(14)^{iii}	O(12)^{iv}		
O(13)	**1.583(8)**	2.54(1)	2.53(1)	2.46(1)		
O(5)^{i}	109.2(4)	**1.518(8)**	2.53(1)	2.49(1)		
O(14)^{iii}	104.3(4)	105.0(4)	**1.578(8)**	2.50(1)		
O(12)^{iv}	111.7(4)	116.6(4)	109.1(4)	**1.474(8)**		
P(3)	O(11)	O(14)	O(15)	O(10)^{iii}		
O(11)	**1.496(8)**	2.55(1)	2.46(1)	2.47(1)		
O(14)	109.4(4)	**1.586(8)**	2.52(1)	2.50(1)		
O(15)	109.9(4)	103.6(4)	**1.551(8)**	2.47(1)		
O(10)^{iii}	117.8(4)	106.1(4)	109.1(4)	**1.486(7)**		
P(4)	O(3)	O(9)	O(8)^{v}	O(15)^{v}		
O(3)	**1.503(8)**	2.48(1)	2.50(1)	2.49(1)		
O(9)	111.9(5)	**1.511(8)**	2.52(1)	2.53(1)		
O(8)^{v}	111.9(4)	114.1(4)	**1.496(8)**	2.47(1)		
O(15)^{v}	105.7(4)	104.1(4)	108.5(4)	**1.617(8)**		

K(1)–O(1)^{vi}	2.848(8)	K(2)–O(1)	2.858(8)
K(1)–O(1)	2.784(8)	K(2)–O(3)	3.354(8)
K(1)–O(2)^{vi}	3.015(8)	K(2)–O(3)^{ii}	2.688(8)
K(1)–O(4)^{ii}	3.018(8)	K(2)–O(4)^{ii}	2.938(8)
K(1)–O(5)	3.078(8)	K(2)–O(6)^{ii}	2.887(7)
K(1)–O(5)^{ii}	2.907(8)	K(2)–O(7)^{iii}	3.113(8)
K(1)–O(6)^{ii}	2.810(7)	K(2)–O(9)	3.092(8)
K(1)–O(9)^{vi}	2.747(8)	K(2)–O(11)	2.704(8)
K(1)–O(10)^{vi}	3.039(7)	K(2)–O(12)	2.754(8)
K(1)–O(12)^{vi}	3.225(8)		
K(1)–O(14)^{vii}	3.344(8)		

Symmetry codes:
i: $-x$; $1/2 + y$; $1/2 - z$
ii: x; $1/2 - y$; $-1/2 + z$
iii: $-3/2 + x$; $3/2 + y$; z
iv: x; $-y - 3/2$; $-3/2 + z$
v: $1/2 - x$; $-y$; $1/2 + z$
vi: $-x$; $-y$; $-z$
vii: $x - 1/2$; $1/2 - y$; $-z$

Note. The V–O or P–O distances are on the diagonal, above it are the O ··· O distances, and below are the O–V–O or O–P–O angles.

$Nb_2O_2P_4O_{13}$ (8) also display an S-shaped configuration of the P_4O_{13} group (Fig. 5c) with three P–O–P angles ranging from 143 to 146°. But this S-shaped geometry does not seem to be the rule for the P_4O_{13} group as shown for $V_6(Si_2O_7)(PO_3)_6(P_4O_{13})$ (6), whose tetraphosphate group exhibits a star-like configuration (Fig. 5d) with P–O–P angles of 151.1°. These results show the extraordinary flexibility of the P_4O_{13} group that should be able to generate numerous original structures.

The geometry of the VO_6 octahedra is characteristic of the vanadyl species; i.e., each octahedron exhibits one abnormally short V–O bond (1.572–1.607 Å), opposed to a very long one (2.227–2.305 Å), and four intermediate equatorial bonds (1.987–2.048 Å).

Two sorts of potassium ions can be distinguished. The K(1) ions that sit at the intersection of the [0 0 1] and [1 0 1] tunnels (Figs. 1 and 4) exhibit an 11-fold coordination, with five nearest neighbors located at distances ranging from 2.747 to 2.907 Å.

The K(2) cations sit in the [1 0 1] tunnels (Fig. 4) near the intersection with the [0 0 1] tunnels (Fig. 1). They are surrounded by nine oxygen atoms, six of which are located at distances ranging from 2.688 to 2.938 Å.

Paramagnetic Behavior of the V(IV) Species

The calculation of the valencies of the atoms using the Brese and O'Keefe theory (9) leads for V(1) and V(2) to the valence states 4.12 and 4.13, respectively. This tetravalent character of vanadium is confirmed by the molar susceptibility measurements. The latter has been fitted with the law $\chi_m = \chi_o + C/(T - \theta)$. The fitting parameter C corresponds to 1.55 μB per V^{IV} ion as expected with the present structure built on isolated $V^{IV}O_6$ octahedra. The $1/\chi_m(T)$ curve in Fig. 6 does not show any indication of magnetic ordering down to 4.5 K in agreement with the fitting value $\theta = 0.6$ K, despite the existence of two independent crystallographic sites of vanadium.

Stability of V(IV) in an Oxidizing Atmosphere

The possibility to grow single crystals of such a phase in air raises the question of the stability of tetravalent vanadium in an oxidizing atmosphere for this particular structure. For this reason a microthermogravimetric analysis of the polycrystalline material, prepared in an evacuated ampoule, was carried out in air and in oxygen flow. Regardless of the atmosphere, no weight increase was observed up to 750°C. At this temperature the compound is melted, but its X-ray diffraction pattern remains unchanged, i.e., characteristic of the $K_2(VO)_2P_4O_{13}$ structure, described above. Only a slight change in color from turquoise to khaki is observed. The magnetic susceptibility measured after thermogravimetric measurements confirmed that vanadium is still in the tetravalent

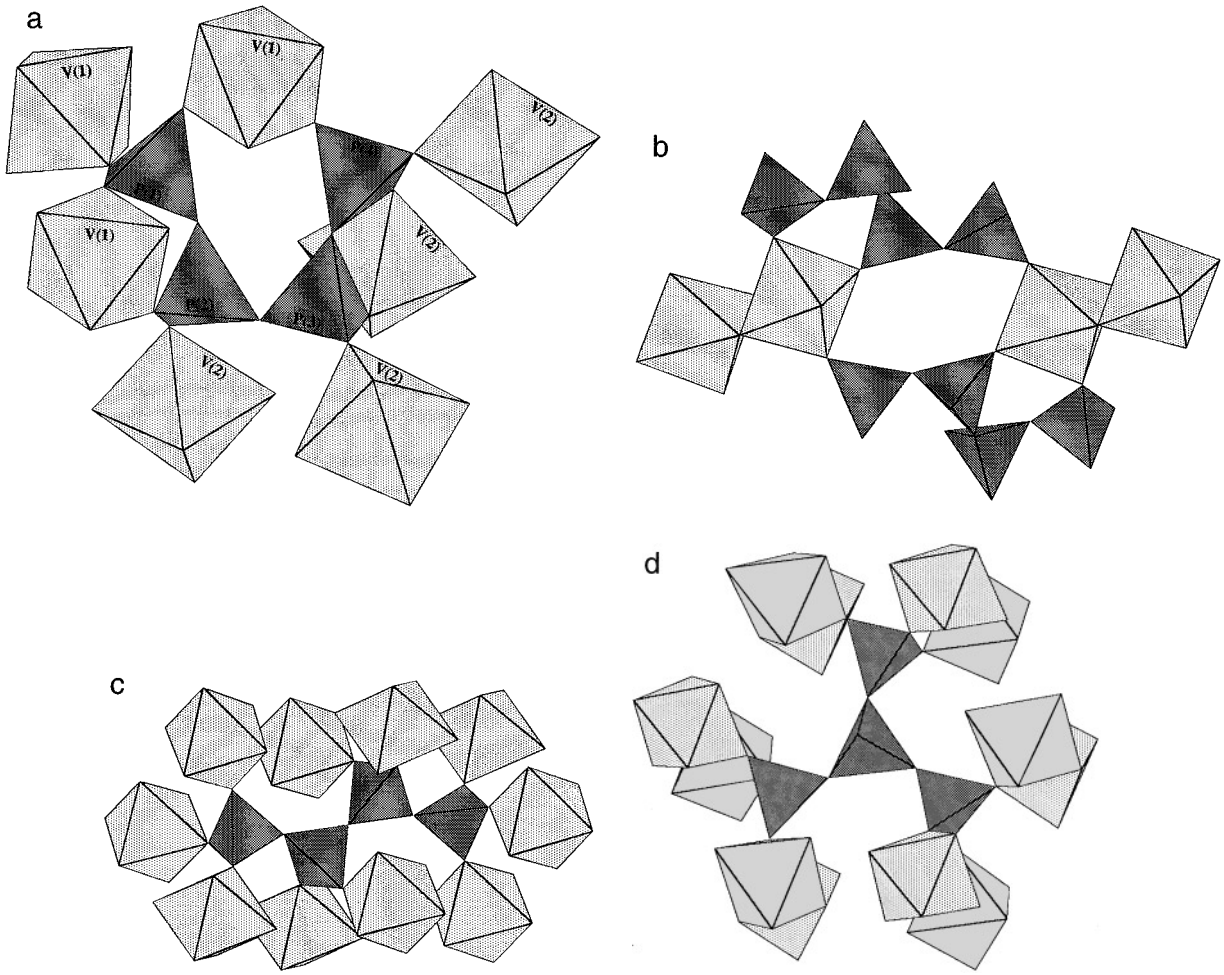

FIG. 5. Configuration of the P_4O_{13} group; (a) in $K_2(VO)_2(P_4O_{13})$, (b) in $KV_4(PO_4)(P_2O_7)(P_4O_{13})$, (c) in $M_2O_2P_4O_{13}$ (M = Nb or Mo), and (d) in $V_6(Si_2O_7)(PO_3)_6(P_4O_{13})$.

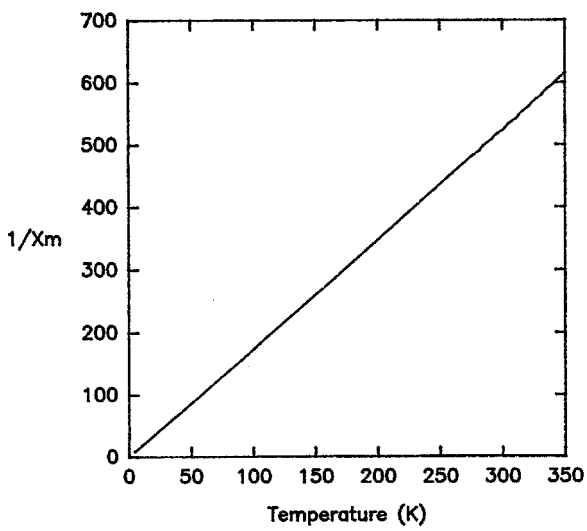

FIG. 6. Inverse of the susceptibility versus the temperature.

state. These results emphasize the exceptional stability of V(IV) in an oxidizing atmosphere, which seems to be specific to phosphates, since the V(IV) oxides are generally oxidized into V(V) by heating in air.

REFERENCES

1. M.-M. Borel, M. Goreaud, A. Grandin, Ph. Labbe, A. Leclaire, and B. Raveau, *Eur. J. Solid State Inorg. Chem.* **28,** 93 (1991).
2. S. Boudin, *Thesis, Caen*, 1996.
3. N. Middlemiss, F. Hawthorne, and C. Calvo, *Can. J. Chem.* **55,** 1673 (1977).
4. B. Klinkert and M. Jansen, *Zeit. Anorg. Allg. Chem.* **567,** 87 (1988).
5. L. Benhamada, G. Grandin, M.-M. Borel, A. Leclaire, and B. Raveau, *J. Solid State Chem.* **104,** 193 (1993).
6. A. Leclaire, H. Chahboun, D. Groult and B. Raveau, *J. Solid State Chem.* **65,** 158 (1986).
7. G. Costentin, A. Leclaire, M.-M. Borel, G. Grandin, and B. Raveau, *Zeit. Kristallogr.* **201,** 53 (1992).
8. N. P. Nikolaev, G. C. Sadikov, A. V. Lavrov, and M. A. Porai-Koshits, *Inorg. Mat.* **22,** 1364 (1986).
9. N. E. Brese and M. O'Keefe, *Acta Crystallogr. B* **47,** 192 (1991).